Physics-based modeling of Antarctic snow and firn density

Eric Keenan[1], Nander Wever[1], Marissa Dattler[2], Jan T. M. Lenaerts[1], Brooke Medley[3], Peter Kuipers Munneke[4], and Carleen Reijmer[4]

[1]Department of Atmospheric and Oceanic Sciences, University of Colorado, Boulder, CO, USA
[2]Department of Atmospheric and Oceanic Sciences, University of Maryland, College Park, MD, USA
[3]Cryospheric Sciences Laboratory, NASA Goddard Space Flight Center, Greenbelt, MD, USA
[4]Institute for Marine and Atmospheric Research, Utrecht University, Utrecht, The Netherlands

Correspondence: Eric Keenan (eric.keenan@colorado.edu)

Abstract. Estimates of snow and firn density are required for satellite altimetry based retrievals of ice sheet mass balance that rely on volume to mass conversions. Therefore, biases and errors in presently used density models confound assessments of ice sheet mass balance, and by extension, ice sheet contribution to sea level rise. Despite this importance, most contemporary firn densification models rely on simplified semi-empirical methods, which are partially reflected by significant modeled density errors when compared to observations. In this study, we present a new, wind-driven, drifting snow compaction scheme that we have implemented into SNOWPACK, a physics-based land surface snow model. We demonstrate high-quality simulation of near-surface Antarctic snow firn density at 122 observed density profiles across the Antarctic ice sheet, as indicated by reduced model biases throughout most of the near-surface firn column when compared to two semi-empirical firn densification models. Because SNOWPACK is physics-based, its performance does not degrade when applied to sites without observations used in the calibration of semi-empirical models, and could therefore better represent firn properties in locations without extensive observations and under future climate scenarios, in which firn properties are expected to diverge from their present state.

1 Introduction

The Antarctic ice sheet (AIS) is the largest freshwater reservoir on Earth, and if melted entirely would raise globally averaged sea level by 58 m (The IMBIE team, 2018). The AIS is contributing to sea level rise via net mass loss, with an increasing rate from 40 ± 9 Gt yr^{-1} in 1979 - 1990 to 252 ± 26 Gt yr^{-1} in 2009 - 2017 (Rignot et al., 2019). In order to quantify ice sheet contribution to sea level rise, glaciologists compute the mass balance (MB), defined as the difference between the grounded ice sheet surface mass balance (SMB) and solid ice discharge across the grounding line (Lenaerts et al., 2019). MB can be estimated by combining satellite altimetry estimates of ice sheet volume change with modeled snow and firn density estimates (e.g. Shepherd et al., 2012; Smith et al., 2020). Similar to MB, spatial variations in SMB can be determined from combined density and radar derived annual snow accumulation estimates (e.g. Medley et al., 2013; Dattler et al., 2019; Kausch et al., 2020). However, in all cases, density estimates represent one of the largest sources of uncertainty (Shepherd et al., 2012; Montgomery et al., 2020) due to an uncertain and simplified representation of snow and firn densification (Alexander et al., 2019; Montgomery et al., 2020), particularly over the low-accumulation interior of ice sheets (Weinhart et al., 2020).

Antarctic new snow density and subsequent densification are known to vary in both space and time and are influenced by,
25 among other factors, local meteorology and drifting snow (Herron and Langway, 1980; Sommer et al., 2018). In particular,
surface snow and firn density are known to be strongly impacted by wind driven compaction, a process hereafter referred
to as drifting snow compaction. Drifting snow occurs up to 75 % of the time in the AIS escarpment zone (Lenaerts et al.,
2012; Palm et al., 2017; van Wessem et al., 2018; Amory and Kittel, 2019), and because of drifting snow redistribution,
precipitating snow particles are not always permanently incorporated into the snowpack at the time or location of precipitation.
30 In fact, observations show that in the high-elevation, dry, and windy areas of the AIS, pockets of fresh snow can be found
alongside snow that is more than one year old (Picard et al., 2019). Including processes such as drifting snow compaction,
snow metamorphism, and compaction due to overburden stress has been shown to improve model representation of polar
snow and firn (van Kampenhout et al., 2017). However, despite this finding, as well as the demonstrated complexity of snow
and firn densification, many AIS MB studies (e.g. Zwally et al., 2015; Smith et al., 2020) rely on relatively simplified semi-
35 empirical models (e.g. Ligtenberg et al., 2011; Li and Zwally, 2011; Medley et al., 2020). Semi-empirical densification models
successfully capture broad regional variability in firn characteristics (van den Broeke, 2008; Ligtenberg et al., 2011). However,
due to their limited complexity, as measured by the inclusion of ephemeral processes such as drifting snow compaction,
they cannot capture all local and temporal density variability. Additionally, semi-empirical models are tuned to observations
representative of the past or present climate (Herron and Langway, 1980; Ligtenberg et al., 2011; Li and Zwally, 2011), which
40 may not be representative under future climate change scenarios (Ligtenberg et al., 2014). Furthermore, because semi-empirical
models rely on extensive tuning to observations, rather than physical principles, they may not perform well in climates poorly
sampled by observations (e.g. the East Antarctic plateau). Alternatively, physics based models, for example CROCUS (Vionnet
et al., 2012) and SNOWPACK (Bartelt and Lehning, 2002; Lehning et al., 2002a, b), do not explicitly tune simulated density
to observations. Instead, physics-based models represent densification using a constitutive relationship between stress and
45 strain for snow. However, physics-based approaches are hindered by a variety of factors including computational expense, the
requirement to estimate unknown parameters such as surface roughness length and snow activation energy, as well as the need
to calculate intermediate prognostic variables including snow grain size and viscosity. Despite these drawbacks, the complex
material properties of snow, combined with an acute scarcity of snow and firn density measurements lead us to hypothesize
that a physics-based modeling approach is preferred.

50 In order to improve model representation of Antarctic snow and firn properties compared to semi-empirical models, we apply
the physics-based snow model, SNOWPACK, to nine automatic weather stations (AWS), 55 borehole 10 m depth temperatures,
and 122 observed near-surface density profiles for a total of 186 locations across the AIS. First, we describe model setup and
a new drifting snow routine designed to improve representation of near-surface (depth ≤ 10 m) snow and firn density (section
2.1). Next, we evaluate SNOWPACK's ability to simulate the surface energy balance by comparing with available surface
55 temperature proxies (section 3.1). We then explore the sensitivity of SNOWPACK simulated density profiles to uncertainties
in atmospheric forcing (section 3.2). Next, we compare SNOWPACK to observed density profiles and compare the relative
performance of SNOWPACK to two other firn densification models (sections 3.3 - 3.6). Finally, we conclude with a more

detailed example of how SNOWPACK can facilitate remote sensing retrieval processing and attribution by describing other simulated snow and firn properties (section 3.7).

2 Methods

2.1 Physics-based snow model SNOWPACK

Many models assume a high ($> 250 \, \mathrm{kg \, m^{-3}}$) new snow density over Antarctica (Ligtenberg et al., 2011; Groot Zwaaftink et al., 2013) despite observational evidence of occasional relatively low ($< 100 \, \mathrm{kg \, m^{-3}}$) new snow density (Groot Zwaaftink et al., 2013; Sommer et al., 2018). This difference can be explained by accumulation of snowfall without sufficient wind speed required for drifting snow compaction to occur. In order to account for this, we implement a new drifting snow compaction routine into the vertical, one-dimensional physics-based land-surface snow model, SNOWPACK (Bartelt and Lehning, 2002; Lehning et al., 2002a, b). Originally designed as an alpine snow cover model capable of describing snow cover properties, including accumulation, densification, temperature, energy balance, and snow microstructure, SNOWPACK has been applied to both ice sheets (Groot Zwaaftink et al., 2013; Van Tricht et al., 2016; Steger et al., 2017; Izeboud et al., 2020; Dunmire et al., 2020). These studies have shown that SNOWPACK is capable of capturing important processes in the ice sheet firn layer, namely accumulation in windy environments, the surface energy balance (SEB), and liquid water retention. However, these studies have not implemented a polar snow accumulation scheme that allows for initial accumulation of low ($< 250 \, \mathrm{kg \, m^{-3}}$) density snow and subsequent drifting snow compaction. Additionally, no previous study has evaluated SNOWPACK simulated near-surface firn density across the entire AIS.

Our new drifting snow compaction routine combines an existing alpine new snow density parameterization with a polar snow compaction routine. In particular, we impose the key physical restraint that drifting snow is required for near-surface compaction in addition to overburden stress compaction. This mechanism has previously been proposed in the literature (Brun et al., 1997) and recently confirmed in both laboratory experiments (Sommer et al., 2017) as well as field observations on the AIS (Sommer et al., 2018). In our scheme, new snowfall is given an initial, typically low (30 - 150 $\mathrm{kg \, m^{-3}}$), density ρ_{new}, Eq. (1), according to the default SNOWPACK alpine new snow density parameterization (Lehning et al., 2002a), which varies as a function of 2 m air temperature T_{2m} (°C), snow surface temperature T_s (°C), relative humidity RH (0 - 1), and 10 m wind speed $U_{10 \, \mathrm{m}}$ ($\mathrm{m \, s^{-1}}$).

$$\rho_{\mathrm{new}} = 70 + 6.5 T_{2m} + 7.5 T_s + 0.26 RH + 13 U_{10 \, \mathrm{m}} - 4.5 T_{2m} T_s - 0.65 T_{2m} U_{10 \, \mathrm{m}} - 0.17 RH U_{10 \, \mathrm{m}} + 0.06 T_{2m} T_s RH \qquad (1)$$

Densification then occurs via two distinct processes, a) densification due to overburden stress and b) densification due to drifting snow compaction. Densification due to overburden stress is calculated nearly identically as described in Steger et al. (2017) which adapted SNOWPACK for use in the percolation zone of the Greenland Ice Sheet by tuning the viscosity parameters including the snow activation energy Q_s and critical exponent β. However, because of better agreement with observed density profiles, we revert to original SNOWPACK viscosity parameters by setting Q_s and β to 67,000 $\mathrm{J \, mol^{-1}}$
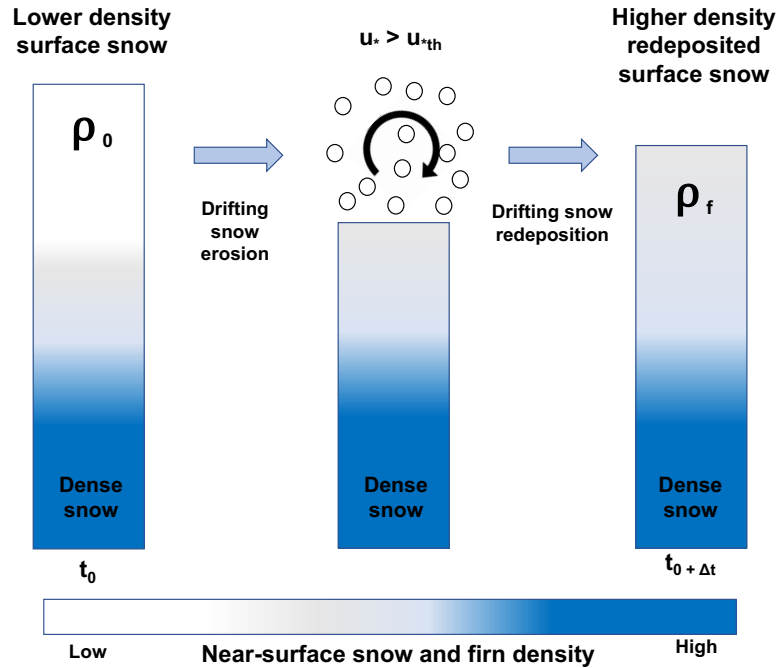
Figure 1. Schematic of SNOWPACK drifting snow compaction. When the friction velocity exceeds the snow threshold friction velocity $(u_* > u_{*th})$, initial lower density surface snow (left) is eroded by the wind, suspended above the snow surface (middle), and then redeposited with a higher density (right).

and 0.7 respectively. The second mechanism driving densification, i.e. drifting snow compaction, occurs when the friction

90 velocity u_* ($\mathrm{m\,s^{-1}}$) exceeds the snow threshold friction velocity u_{*th} ($\mathrm{m\,s^{-1}}$) (Fig. 1). In our implementation of SNOWPACK, u_* is estimated by scaling hourly averaged 10 m wind speeds from MERRA-2 atmospheric reanalysis (section 2.2) using a logarithmic wind profile (Lehning et al., 2002a) with a roughness length, z_0, of 2 mm. Meanwhile, u_{*th}, Eq. (2), is calculated as a function of of snow microstructural properties internally determined by SNOWPACK, including snow grain sphericity SP (0 - 1), radius r_g (m), bond radius r_b (m), and coordination number N_3 (Lehning and Fierz, 2008).

95 $$u_{*th} = \sqrt{\frac{A\rho_i g r_g (SP+1) + B\sigma N_3 \frac{r_b^2}{r_g^2}}{\rho_a}} \qquad (2)$$

In Eq. (2), ρ_i is the density of ice (917 $\mathrm{kg\,m^{-3}}$), ρ_a is the density of air (1.1 $\mathrm{kg\,m^{-3}}$), g is the gravitational acceleration (9.8 $\mathrm{m\,s^{-2}}$), σ is a reference shear strength set to 300 Pa, while constants A and B are set to 0.02 and 0.0015 respectively. When u_* exceeds u_{*th}, a saltation mass transport rate Q ($\mathrm{kg\,m^{-1}\,s^{-1}}$) is calculated following Lehning and Fierz (2008) and

then scaled to a drifting snow mass flux Φ ($\mathrm{kg\,m^{-2}\,s^{-1}}$), Eq. (3), by dividing Q by a characteristic horizontal length scale L.

$$\Phi = \frac{Q}{L} = \frac{0.0014\rho_a u_*(u_* - u_{*\mathrm{th}})(u_* + 7.6u_{*\mathrm{th}} + 205)}{L} \qquad (3)$$

L can be interpreted as a fetch length and characteristic horizontal length scale over which the originally upwind and now mobilized snow particles, accounted for in the drifting snow mass flux Φ, are distributed before erosion. We choose a magnitude for L of 10 m, as this is a typical horizontal length scale of wind erosion features including sastrugi and barchan dunes (Filhol and Sturm, 2015). Given a lack of direct observations, L can effectively be considered a tuning parameter, whose magnitude is inversely proportional to Φ. Note that as suspension of drifting snow cannot be properly resolved by a one-dimensional snow model (Lehning and Fierz, 2008), the saltation mass transport rate Q and subsequent drifting snow mass flux Φ are intended to account for all wind driven snow transport processes (i.e. saltation and suspension).

Following drifting snow erosion, the drifting snow mass flux is redeposited at the snow surface with an updated density $\rho_{\mathrm{redeposit}}$ ($\mathrm{kg\,m^{-3}}$), Eq. (4), parameterized according to field measurements of fresh surface snow deposited during drifting snow events (Groot Zwaaftink et al., 2013, equation 1). Note that, in contrast to Groot Zwaaftink et al. (2013), which uses 100-hour average wind speeds, we calculate $\rho_{\mathrm{redeposit}}$ using hourly mean MERRA-2 10 m wind speeds. We implement this distinction in order to better resolve the temporal evolution of redeposited snow density during ephemeral (i.e. shorter than 100 hours) drifting snow events.

$$\rho_{\mathrm{redeposit}} = \begin{cases} 361\log_{10}(U_{10\,\mathrm{m}}) + 33 & U_{10\,\mathrm{m}} > 1\,\mathrm{m\,s^{-1}} \\ 33 & U_{10\,\mathrm{m}} \leq 1\,\mathrm{m\,s^{-1}} \end{cases} \qquad (4)$$

2.2 SNOWPACK atmospheric forcing

At the snow surface, we force SNOWPACK with 1980 - 2017 MERRA-2 global atmospheric reanalysis (Gelaro et al., 2017) hourly mean 2 m air temperature, relative humidity, 10 m wind speed, incoming shortwave and longwave radiation (ISWR and ILWR), and precipitation rate. At the bottom of the simulated snowpack, we apply the MERRA-2 1980 - 2017 mean annual surface temperature as a thermodynamic boundary condition. We choose MERRA-2 because it provides a low release latency (approximately one month) and publicly available description of the state of the atmosphere, whereas regional climate models are not always regularly updated. Additionally, Medley and Thomas (2019) reported MERRA-2 to have the lowest accumulation bias compared to observations among comparable reanalysis products. Furthermore, Gossart et al. (2019) reports generally good agreement between MERRA-2 and observed near surface climatology, including 2 m air temperature and wind speeds, however MERRA-2 appears to overestimate SMB, with a mean absolute error of $58.5\,\mathrm{kg\,m^{-2}\,yr^{-1}}$.

We evaluate MERRA-2 atmospheric reanalysis as forcing for SNOWPACK by comparing with monthly averaged observations at nine AWS, whose locations are shown in Fig. 2. The AWS measure temperature, relative humidity, wind speed and direction, air pressure, and the full radiation balance, i.e. incoming and reflected short wave radiation, and incoming and outgoing longwave radiation. Data from these stations are presented in Reijmer (2002) and Jakobs et al. (2020) and have been previously used to evaluate remote sensing retrievals (Trusel et al., 2013), ice core paleoclimate records (Medley et al., 2018),
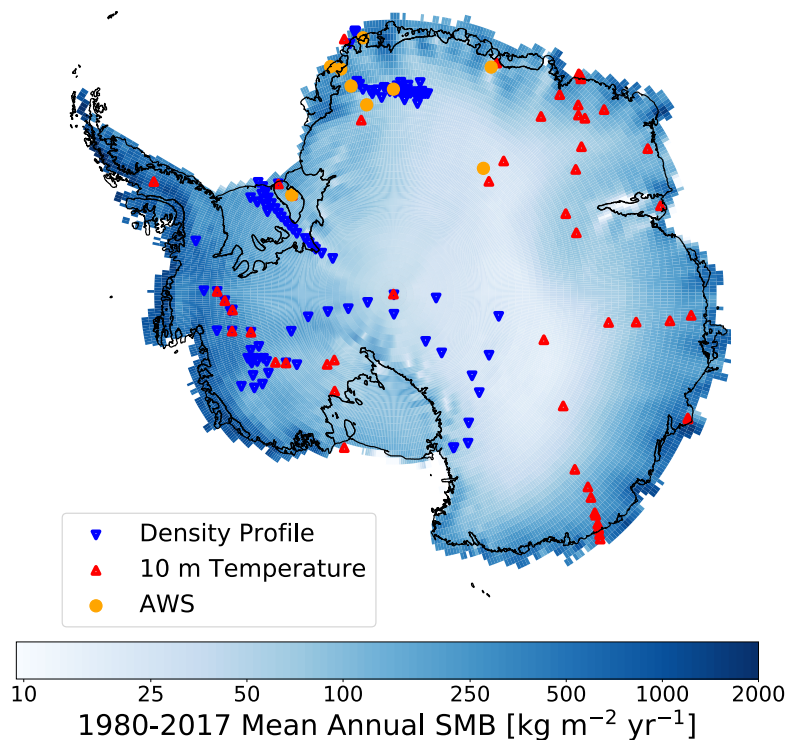
Figure 2. Map of SNOWPACK simulations over the Antarctic ice sheet. Locations of SNOWPACK simulations at 122 observed density profiles (upside down blue triangles), 55 borehole 10 m temperature measurements (red triangles), and nine automatic weather stations (AWS, yellow circles) plotted over MERRA-2 1980 - 2017 mean annual SMB.

130 and climate models (van Wessem et al., 2018). In general, MERRA-2 well captures observed 2 m air temperature, relative humidity, and wind speed, but significantly underestimates both ISWR and ILWR. We calculated an average MERRA-2 bias across all nine AWS of -15.1 $\mathrm{W\,m^{-2}}$ and -16.9 $\mathrm{W\,m^{-2}}$ for ISWR and ILWR, respectively (Fig. A1). In order to reduce this bias in incoming radiation and thus better capture AWS observations, we increase MERRA-2 ISWR by 19.4 % and ILWR by 16.9 $\mathrm{W\,m^{-2}}$. Following bias correction, MERRA-2 ISWR and ILWR biases are reduced to 8.7 $\mathrm{W\,m^{-2}}$ and -0.6 $\mathrm{W\,m^{-2}}$,

135 respectively. Additionally, root mean squared error (RMSE) ISWR is reduced from 22.7 $\mathrm{W\,m^{-2}}$ to 20.3 $\mathrm{W\,m^{-2}}$ while ILWR RMSE is reduced from 21.5 $\mathrm{W\,m^{-2}}$ to 14.1 $\mathrm{W\,m^{-2}}$. Note that this bias correction only impacts ISWR and ILWR forcing, not 2 m air temperature, relative humidity, 10 m wind speed, and precipitation rate. Additionally, for the rest of this study, all simulations are driven by bias corrected ISWR and ILWR, unless explicitly stated otherwise.

2.3 SNOWPACK model spinup

140 In order to ensure a realistic representation of snow and firn properties throughout the entire near-surface, we complete a SNOWPACK model spinup such that simulated snow depth is 10 m at each site before comparison with observations. We

choose 10 m in order to resolve seasonal variability in snow and firn characteristics as well as energy exchange with the atmosphere. For spinup, we mimic the method presented in Ligtenberg et al. (2011) by repeating the 1980 - 2017 model period until initial simulated snow depth on January 1st, 1980 is at least 10 m. Once spinup is complete, we perform one final 1980 -
145 2017 model simulation.

2.4 Borehole 10 m temperature as mean annual surface temperature proxy

To test MERRA-2 and SNOWPACK's ability to capture the SEB across a range of AIS surface climates, we compare 1980 - 2017 mean MERRA-2 surface temperature and SNOWPACK snow surface temperature with 10 m depth temperatures from 55 boreholes whose locations are show in Fig. 2. In the absence of significant surface meltwater percolation, 10 m depth
150 temperature equilibrates with mean annual surface temperature, and can therefore be used as a proxy for surface temperature and by extension SEB in the absence of direct observations (van den Broeke, 2008; Lenaerts et al., 2012; van Wessem et al., 2014).

2.5 IMAU-FDM firn densification model

To aid in the evaluation of SNOWPACK modeled near-surface density, we also compare with the widely used Institute for Ma-
155 rine and Atmospheric research Utrecht firn densification model (IMAU-FDM v1.1) (Ligtenberg et al., 2011; Kuipers Munneke et al., 2015; Ligtenberg et al., 2018). The IMAU-FDM is a semi-empirical firn densification model designed to represent snow and firn cover processes including densification, meltwater refreezing and percolation, and surface height change. Gridded IMAU-FDM density profiles are available at 27 km horizontal, 4 cm vertical, and 30 day temporal resolution with atmospheric forcing provided by the regional climate model RACMO 2.3p2 (van Wessem et al., 2018)

160 ## 2.6 GSFC-FDM firn densification model

In addition to IMAU-FDM we also compare SNOWPACK to the NASA Goddard Space Flight Center firn densification model (GSFC-FDMv1) which provides simulated firn properties over the past 40 years (1980 - 2019) for both the Greenland and Antarctic ice sheets (Medley et al., 2020). GSFC-FDM uses the Community Firn Model, a modular, open-source framework for Lagrangian modeling of several firn and firn-air related processes within a single column (Stevens et al., 2020). The GSFC-
165 FDM simulations are forced by an enhanced resolution hybridized MERRA-2 that was developed by exploiting a 15-year, 12.5 km resolution offline MERRA-2 replay. The hybridized MERRA-2 forcing retains the spatial gradients in the high-resolution replay while maintaining the temporal variations from the original MERRA-2 variables. The dry snow and firn compaction model, based on Arthern et al. (2010), was calibrated to observed depth-density profiles from both Greenland and Antarctica. A simple initial density scheme was implemented based on mean annual MERRA-2 climate, which provides a spatially variable
170 initial density that does not, however, vary in time.

2.7 SNOWPACK comparison with density observations, IMAU-FDM, and GSFC-FDM

We evaluate SNOWPACK's skill in representing surface and near-surface snow and firn density, defined here as depths of 0 - 1 m and 0 - 10 m, respectively, by comparing with community sourced and publicly available density profiles from the Surface Mass Balance and Snow on Sea Ice Working Group (SUMup) data set (Albert, 2007; Medley et al., 2013; Montgomery et al., 2018) and the firn densification models IMAU-FDM and GSFC-FDM, both of which have been used in satellite altimetry based MB studies (Shepherd et al., 2012; Smith et al., 2020). We first identified all available Antarctic SUMup density observations in the near-surface and then retrieved spatially and temporally consistent SNOWPACK, IMAU-FDM, and GSFC-FDM model output. This classification yielded 122 unique observed profiles (Fig. 2) that are located primarily on the grounded ice sheet, where surface melt is absent or very rare. Observations and models report different vertical resolution density, therefore we compute the mean and standard deviation of all 122 density profiles at ten 1 m thick vertical levels, beginning at 0 - 1 m and ending with 9 - 10 m depths.

3 Results and Discussion

3.1 Surface energy balance

The large variability in observed 10 m depth borehole temperatures, ranging from -57.0 to -14.4 °C, is well captured by MERRA-2, non-bias corrected SNOWPACK, and bias corrected SNOWPACK, indicating proper representation of average SEB (Fig. 3). In particular, the R-squared values and slope of linear regressions are 0.96 and 1.00 for MERRA-2, 0.97 and 0.98 for non-bias corrected SNOWPACK, and 0.97 and 0.95 for bias corrected SNOWPACK, respectively. MERRA-2 overestimates T_s, with an average bias of 0.52 °C, while non-bias corrected SNOWPACK underestimates T_s with an average bias of -0.99 °C. Meanwhile, bias corrected SNOWPACK yields almost perfect agreement, with an average bias of 0.06 °C. MERRA-2 shows the largest RMSE, 2.38 °C, while the non-bias corrected and bias corrected versions of SNOWPACK display an RMSE of 2.16 and 1.94 °C, respectively.

Since the MERRA-2 bias in ISWR and ILWR is determined using only 9 AWS located primarily in Dronning Maud Land (section 2.2), we were initially concerned with the bias' spatial representativeness. However, following bias correction, the reduction in both RMSE and bias ($p < 0.01$) magnitude when compared to 10 m depth temperatures, indicates a clear improvement in SNOWPACK's representation of Antarctic SEB.

3.2 SNOWPACK density profiles sensitivity to atmospheric forcing uncertainty.

Although we've performed an evaluation of MERRA-2 SEB, and introduced a bias correction for ISWR and ILWR, uncertainties is bias-corrected MERRA-2 atmospheric forcing likely still exist, and can impact simulated density profiles. To understand the effect of these uncertainties on SNOWPACK simulated density, we perform an ensemble of SNOWPACK simulations at South Pole and the West Antarctic Ice Sheet divide (WAIS), where we perturb MERRA-2 prescribed 10 m wind speed, 2 m air temperature, and precipitation. Because MERRA-2 exhibits mean absolute errors of 2.4 m s^{-1} and 3.1 °C for annual average
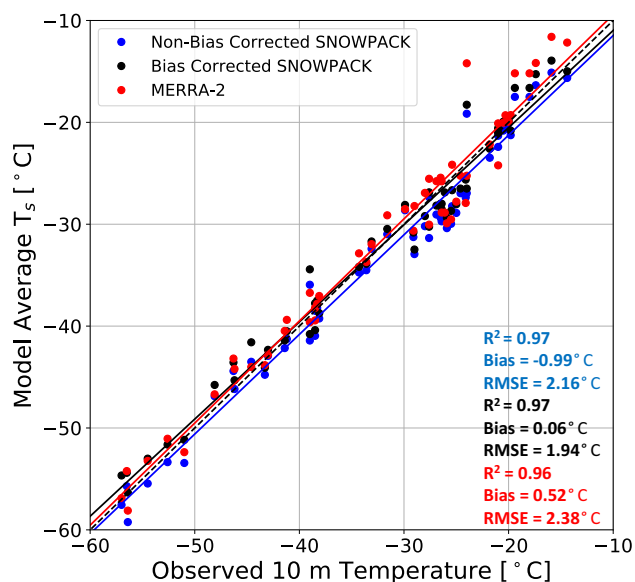
Figure 3. Modeled surface temperature evaluation. Comparison between observed borehole 10 m depth temperature (°C) and 1980 - 2017 model average non-bias corrected SNOWPACK (blue), bias corrected SNOWPACK (black), and MERRA-2 (red) surface temperature T_s (°C). The dashed black line represents a one to one line. Solid lines represent linear regressions. R-squared values, mean bias, and RMSE are reported for non-bias corrected SNOWPACK (blue text), bias corrected SNOWPACK (black text), and MERRA-2 (red text).

10 m wind speeds and near-surface temperature (Gossart et al., 2019) and typical relative accumulation errors of 20 % (Medley and Thomas, 2019), we independently increase and decrease MERRA-2 10 m wind speed, 2 m air temperature, and precipitation at South Pole and WAIS by $2.4 \, \mathrm{m \, s^{-1}}$, 3.1 °C, and 20 %, respectively. SNOWPACK simulated density sensitivities to uncertainties in 10 m wind speed are considerably larger than that of 2 m air temperature and precipitation and range from -46.6 $\mathrm{kg \, m^{-3}}$ at 0 - 1 m in the South Pole - $2.4 \, \mathrm{m \, s^{-1}}$ simulation to 58.5 $\mathrm{kg \, m^{-3}}$ at 2 - 3 m in the WAIS + $2.4 \, \mathrm{m \, s^{-1}}$ simulation (Fig. 4). Meanwhile, across our 2 m air temperature and precipitation ensemble, differences in simulated density are generally small, less than 5 % of non-perturbed density in 75 out of 80 cases, and never exceed 10 %. Because these simulated density differences are typically small compared absolute density, we conclude that uncertainties arising due to 2 m air temperature and precipitation alone are smaller in magnitude than uncertainties arising from firn densification model choice (sections 3.3 - 3.5). Alternatively, density differences in the 10 m wind speed experiments are larger, particularly from 0 - 3 m depth, and exceed 5 % of non-perturbed density in 24 out of 40 cases. In the context of our study, simulated density uncertainties arising from uncertainties in MERRA-2 wind speed cannot be easily reduced because, consistent with Gossart et al. (2019), we
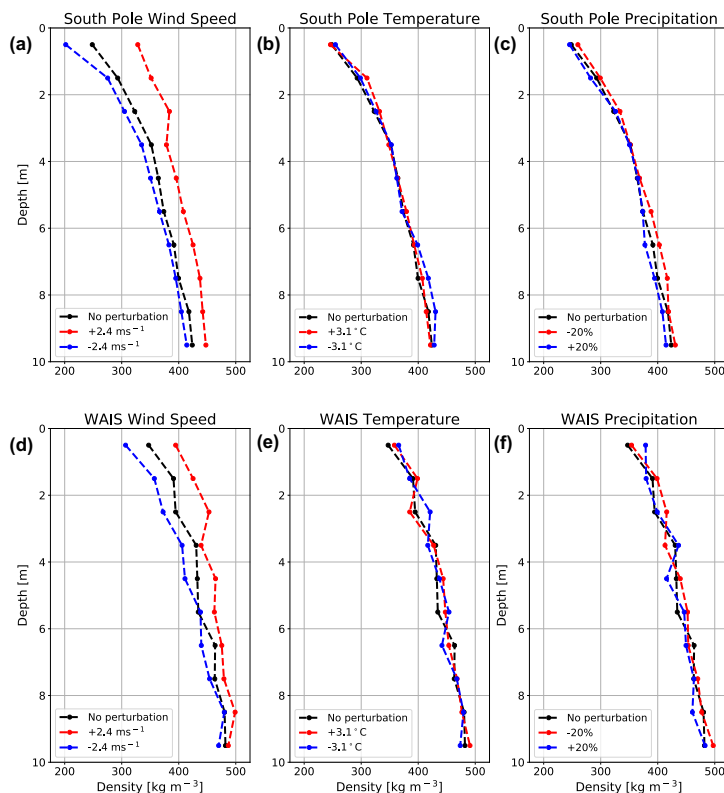
Figure 4. SNOWPACK simulated density profile sensitivity to uncertainties in atmospheric forcing. SNOWPACK simulated density profile sensitivity at South Pole (a,b,c) and WAIS (d,e,f), to wind speed (a,d), temperature (b,e), and precipitation (c,f). The increased wind speed (+ 2.4 $\mathrm{m\,s^{-1}}$), increased temperature (+ 3.1 °C), and reduced precipitation (- 20 %) perturbations are shown in red, while decreased wind speed (- 2.4 $\mathrm{m\,s^{-1}}$), decreased temperature (- 3.1 °C), and increased precipitation (+ 20 %) perturbations are shown in blue. In all panels, density profiles are valid for December 31st, 2017 and black curves represents unperturbed atmospheric forcing simulations.

find no consistent bias in MERRA-2 wind speed compared to observations (section 2.2). We must therefore acknowledge that

215 wind speed represents the largest source of uncertainty with regard to SNOWPACK simulated near-surface density, and in fact, exceeds uncertainties arising from firn densification model choice.

3.3 Surface snow density

A comparison between both SNOWPACK, IMAU-FDM, and GSFC-FDM simulated surface snow density, defined as the top meter, with 79 unique observations is shown in Fig. 5. Observations range from 272 - 507 $\mathrm{kg\,m^{-3}}$, with a mean of 362 $\mathrm{kg\,m^{-3}}$

220 and standard deviation of 39 $\mathrm{kg\,m^{-3}}$. Since it is known that meteorological conditions including annual accumulation and temperature influence Antarctic snow and firn density (Herron and Langway, 1980), we tested for explanatory variables. We

find a modest relationship between MERRA-2 1980 - 2017 mean annual SMB and observed surface snow density (p < 0.001, R^2 = 0.23) as well as a significant, but weak correlation between elevation and observed surface snow density (p < 0.001, R^2 = 0.16), likely due to the relationship between elevation and surface climate. Note that, perhaps surprisingly, we find no

225 significant correlation between MERRA-2 1980 - 2017 mean wind speed and observed surface density (p = 0.14, R^2 = 0.03). Because drifting snow compaction is known to partially control snow density on daily to hourly timescales (Sommer et al., 2018), the lack of a significant relationship between mean annual wind speed and surface snow density indicates the importance of resolving drifting snow compaction with high temporal resolution (daily to hourly) meteorological forcing as opposed to annual means or climatology.

230 SNOWPACK (linear fit slope = 0.51, R^2 = 0.20), IMAU-FDM (linear fit slope = 0.20, R^2 = 0.19), and GSFC-FDM (linear fit slope = 0.22, R^2 = 0.36) all modestly capture observed surface snow density variability. Both SNOWPACK and IMAU-FDM underestimate surface snow density with an average bias of -8.2 and -20.4 $\mathrm{kg\,m^{-3}}$ and RMSE of 45.3 and 40.7 $\mathrm{kg\,m^{-3}}$, respectively. Meanwhile GSFC-FDM, on average overestimates surface snow density, with a bias of 20.4 $\mathrm{kg\,m^{-3}}$ and RMSE of 38.5 $\mathrm{kg\,m^{-3}}$. For all models, we identify no clear relationship between geographic location and model bias. However, we

235 find a significant but weak negative relationship between observed density and modeled surface density bias for SNOWPACK (p < 0.001, R^2 = 0.19) as well as a moderately strong negative relationship for IMAU-FDM (p < 0.001, R^2 = 0.80) and strong negative relationship for GSFC-FDM (p < 0.001, R^2 = 0.87).

According to our analysis, SNOWPACK better captures the range in observed surface density when compared to IMAU-FDM, as evidenced by a lower magnitude bias, higher R^2, and a linear fit slope closer to unity, but the typical error is larger,

240 as expressed by a slightly larger RMSE. Likewise, when compared to GSFC-FDM, SNOWPACK exhibits a lower surface density bias magnitude and has a linear slope closer to unity, but exhibhits a larger RMSE and lower R^2. Additionally, we calculate a p-value of 0.06 for a two-sided test in which the null hypothesis states that SNOWPACK and IMAU-FDM have identical average biases. This information combined with SNOWPACK's larger RMSE compared to IMAU-FDM and GSFC-FDM, and smaller R^2 compared to GSFC-FDM, leads us to conclude that neither model is superior, and instead that all

245 three models perform comparably with regard to surface density. Note that all three models perform particularly poorly when observed surface density exceeds 400 $\mathrm{kg\,m^{-3}}$ (SNOWPACK: Bias = -23.7 $\mathrm{kg\,m^{-3}}$, RMSE = 65.8 $\mathrm{kg\,m^{-3}}$; IMAU-FDM: Bias = -65.4 $\mathrm{kg\,m^{-3}}$, RMSE = 74.7 $\mathrm{kg\,m^{-3}}$; GSFC-FDM: Bias = -20.4 $\mathrm{kg\,m^{-3}}$, RMSE = 35.6 $\mathrm{kg\,m^{-3}}$). The origin of this poor performance at high observed surface densities is not known for certain, and likely cannot be explained by topographic slope as we find no significant relationship between surface slope derived from a 1 km horizontal resolution digital elevation model

250 (Helm et al., 2014) and modeled surface density bias. Alternatively, this model degradation at high observed surface densities could potentially be explained by an underestimation of new snow density and/or the frequency/intensity of simulated drifting snow compaction due to the presence local meteorological phenomena not captured by MERRA-2 or RACMO2. Additionally, we cannot rule out model degradation at high observed densities due to errors in the observations themselves. For example, some surface density observations, particularly those from deep firn and ice cores, may not be representative of an undisturbed

255 snow surface and could therefore report an artificially high surface density. Moreover, surface snow samples taken from cores
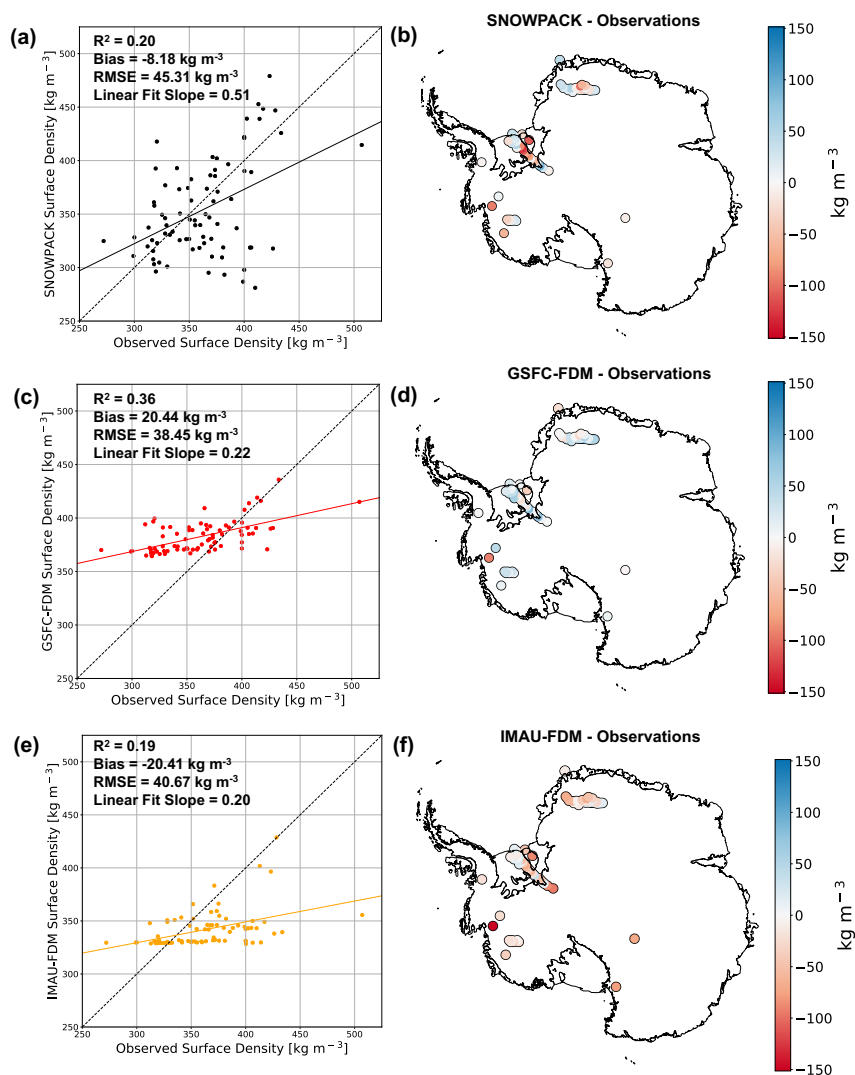
Figure 5. Modeled and observed surface density comparison. Scatter plot of observed vs. SNOWPACK modeled surface density at 79 locations across the AIS (a). Scatter plot of observed vs. GSFC-FDM modeled surface density at 79 locations across the AIS (c). Scatter plot of observed vs. IMAU-FDM modeled surface density at 79 locations across the AIS (E). Map of SNOWPACK minus observed surface density at 79 locations across the AIS (b). Map of GSFC-FDM minus observed surface density at 79 locations across the AIS (d). Map of IMAU-FDM minus observed surface density at 79 locations across the AIS (f). In panels a, c, and e, dashed black lines represent one to one lines while solid lines represent linear regressions.

are often compressed by the drill and can sometimes break into multiple pieces, therefore confounding density measurements. Finally, simulated surface density errors could be explained by uncertainties in MERRA-2 10 m wind speeds (section 3.2).

3.4 Near-surface snow and firn densification

In a comparison at 122 unique observed density profiles, SNOWPACK, when compared to IMAU-FDM, exhibits a lower mean
260   density bias magnitude throughout the entire near-surface, and when compared to GSFC-FDM from 0 - 7 m depth (Fig. 6).
Observed mean densities range from 362 $\mathrm{kg\,m^{-3}}$ at depth 0 - 1 m to 510 $\mathrm{kg\,m^{-3}}$ at 9 - 10 m. Meanwhile, SNOWPACK mean
densities range from 354 $\mathrm{kg\,m^{-3}}$ at depth 0 - 1 m to 489 $\mathrm{kg\,m^{-3}}$ at 9 - 10 m. SNOWPACK underestimates observed density
at depth with biases varying from a minimum of -0.6 $\mathrm{kg\,m^{-3}}$ at depth 2 - 3 m to a maximum of -25.3 $\mathrm{kg\,m^{-3}}$ at 8 - 9 m.
Note that SNOWPACK mean density bias magnitudes from 0 - 7 m are typically small ($< 10\ \mathrm{kg\,m^{-3}}$), and are approximately
265   the same magnitude as uncertainties arising from uncertainties in atmospheric forcing (Section 3.2). The IMAU-FDM likewise
underestimates near surface density with biases ranging from -20.4 $\mathrm{kg\,m^{-3}}$ at depth 0 - 1 m to -40.1 $\mathrm{kg\,m^{-3}}$ at 8 - 9 m.
Meanwhile, GSFC-FDM overestimates surface density with biases ranging from 8.5 $\mathrm{kg\,m^{-3}}$ at depth 8 - 9 m to 23.7 $\mathrm{kg\,m^{-3}}$
at 2 - 3 m. Furthermore, SNOWPACK correctly predicts observed variability in mean density, as shown by similar standard
deviations between SNOWPACK and observations (Fig. 6, panel A). Alternatively, the IMAU-FDM and GSFC-FDM both
270   underestimate observed mean density variability at the surface, but converge towards the observed variability with increasing
depth.

To test for the potential effect of compensating biases on our analysis of near-surface densification, we partition the 122
observed density profiles into 35 high SMB and 87 low SMB categories based off a MERRA-2 mean annual SMB threshold of
200 $\mathrm{kg\,m^{-2}\,yr^{-1}}$ (Fig. 7). We choose 200 $\mathrm{kg\,m^{-2}\,yr^{-1}}$ because it roughly approximates the area weighted mean annual SMB
275   over the grounded AIS (172.8 $\mathrm{kg\,m^{-2}\,yr^{-1}}$ according to Agosta et al. (2019)). Again, for both high and low SMB sites, we find
that SNOWPACK, when compared to IMAU-FDM, shows reduced mean density bias throughout the entire near-surface firn
column, from the surface down to 10 m depth. While compared to GSFC-FDM, SNOWPACK exhibits a reduced near-surface
density bias only from 0 - 8 m and 9 - 10 m at low accumulation sites. Note generally good agreement between SNOWPACK
and observations at both high and low SMB sites. For high SMB sites, SNOWPACK mean biases range from -55.9 $\mathrm{kg\,m^{-3}}$ at
280   8 - 9 m to -3.9 $\mathrm{kg\,m^{-3}}$ at 0 - 1 m, while for low SMB sites, mean biases are generally reduced in magnitude and range from
-14.3 $\mathrm{kg\,m^{-3}}$ at 9 - 10 m to 8.3 $\mathrm{kg\,m^{-3}}$ at 5 - 6 m. Given SNOWPACK's mean bias reduction, when compared to IMAU-FDM,
and comparable peformance relative to GSFC-FDM, we have demonstrated our physics-based modeling approach is capable
of reliably capturing Antarctic near-surface snow and firn density.

3.5 Simulated near surface firn densification at sites not included in GSFC-FDM model calibration

285   Semi-empirical firn densification models, including IMAU-FDM and GSFC-FDM, are calibrated against observed density pro-
files in order to improve model agreement with observations. However, because near-surface density observations are sparse,
not evenly distributed in space, and typically collected in summer, semi-empirical models may be biased towards climate
regimes which are well sampled by observations. Alternatively, SNOWPACK, and other physics-based models, simulate den-
sity profiles which are not calibrated against observations and could therefore, potentially outperform semi-empirical models
290   in climate regimes not well sampled in semi-empirical model calibrations. To test this hypothesis, we examine the 69 of 122
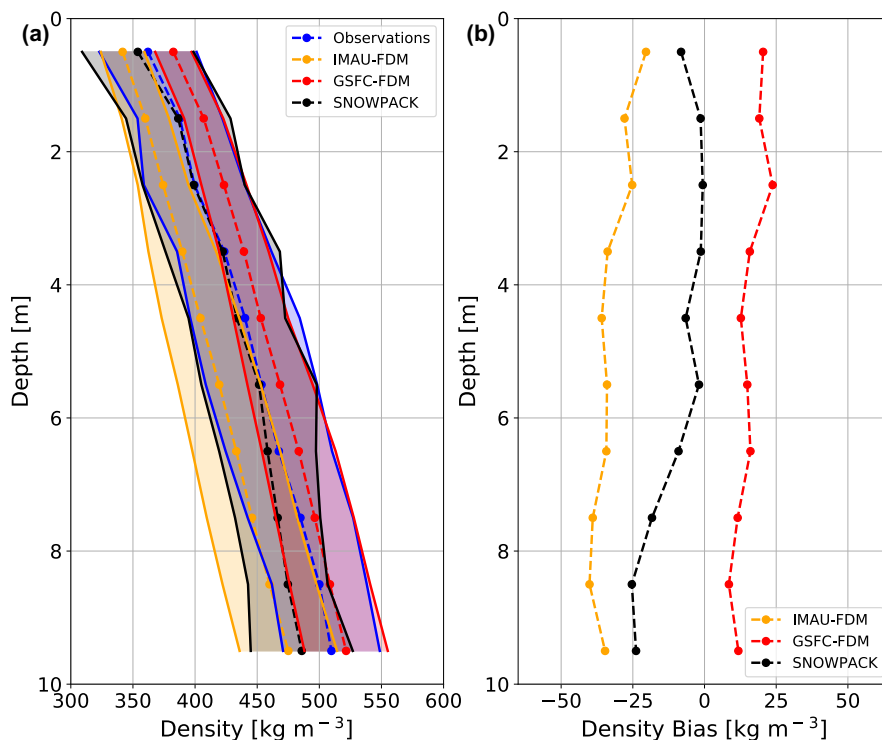
Figure 6. Density profile comparison. Mean observed (blue dashed), SNOWPACK modeled (black dashed), GSFC-FDM (red dashed) and IMAU-FDM modeled (yellow dashed) near surface (0 - 10 m) density profiles at 122 locations across the AIS (a). Shading represents plus and minus one standard deviation across observed and modeled density profiles. Mean SNOWPACK minus observed (black dashed), GSFC-FDM minus observed (red dashed), and IMAU-FDM minus observed (yellow dashed) density profiles at 122 locations across the AIS (b).

observed denstiy profiles which were not included in the GSFC-FDM calibration, hereafter refered to as the 69 independent sites. We then compare the mean near-surface density biases of SNOWPACK and GSFC-FDM at these 69 independent sites against the same statistics calculated for all 122 sites (Section 3.4). Unfortunately, we do not know which of the 122 observed density profiles were used in the IMAU-FDM calibration, therefore we exclude IMAU-FDM from this analysis.

295   By examining only the 69 independent sites, mean GSFC-FDM density bias magnitudes increase throughout the near-surface compared to all 122 sites, on average by $6.9 \, \mathrm{kg \, m^{-3}}$, whereas the mean SNOWPACK density bias magnitude remains nearly unchanged, increasing by only $0.02 \, \mathrm{kg \, m^{-3}}$ (Fig. 8). Because the mean near-surface density bias increases for GSFC-FDM while remaining nearly the same for SNOWPACK, we conclude that semi-empirical firn densification models exhibit reduced model performance at sites not included in density calibration, whereas SNOWPACK does not demonstrate a significant change

300   in model accuracy.
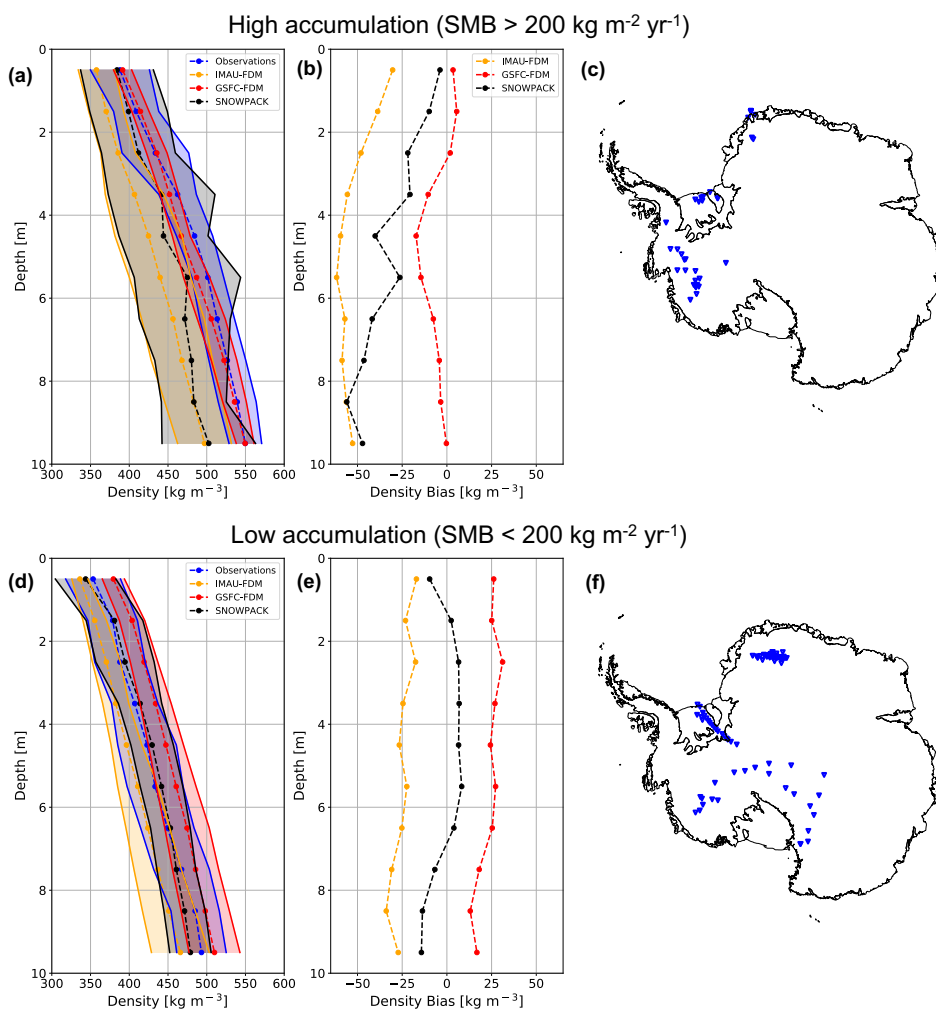
Figure 7. High and low SMB density profile comparison. Average observed (blue dashed), SNOWPACK modeled (black dashed), GSFC-FDM modeled (red dashed), and IMAU-FDM modeled (yellow dashed) near surface (0 - 10 m) density profiles at high (a) and low (d) SMB sites. Shading represents plus and minus one standard deviation across observed and modeled density profiles. Mean SNOWPACK minus observed (black dashed), GSFM-FDM minus observed (red dashed), and IMAU-FDM minus observed (yellow dashed) at high (b) and low (e) SMB sites. Maps of locations of high (c) and low (f) SMB sites. High and low SMB sites are delineated by a MERRA-2 1980 - 2017 mean annual SMB threshold of 200 $kg\,m^{-2}\,yr^{-1}$.

3.6 SNOWPACK and semi-empirical models hierarchical complexity

Although all three models are presented on similar footing, it is important to contextualize their performance by noting the different original purposes for developing SNOWPACK, IMAU-FDM, and GSFC-FDM, as well as their different level of process representation complexity. The IMAU-FDM and GSFC-FDM are relatively simplified semi-empirical firn models
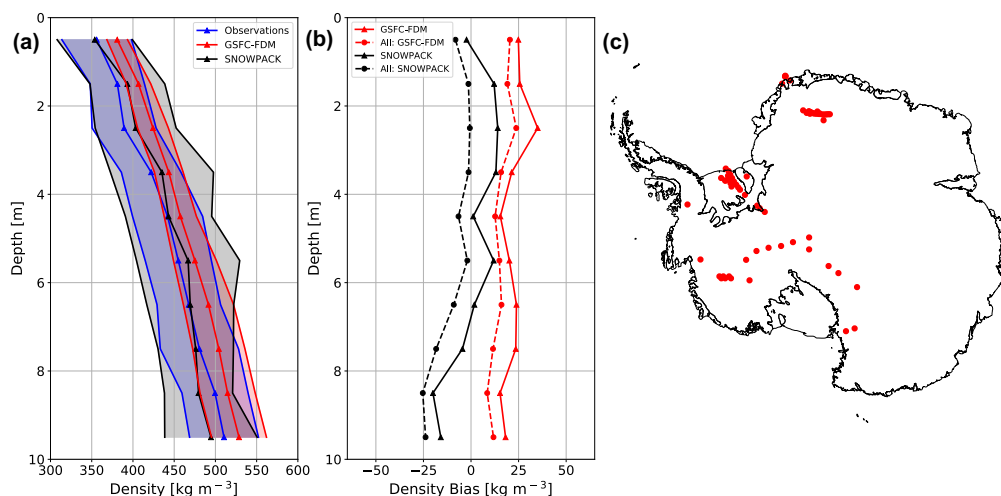
Figure 8. SNOWPACK and GSFC-FDM density simulation at sites not included in GSFC-FDM calibration. Average observed (blue triangles), SNOWPACK modeled (black triangles), and GSFC-FDM modeled (red triangles) near surface (0 - 10 m) density profiles at 69 sites not included in the GSFC-FDM density calibration (a). Shading represents plus and minus one standard deviation across 69 observed and modeled density profiles. Mean SNOWPACK minus observed (black) and GSFC-FDM minus observed (red) density profiles at the 69 of 122 sites not included in the GSFC-FDM density calibration (solid with triangles) and all 122 observed density profiles (dashed with circles, b). Map of 69 observed density profiles not included in the GSFC-FDM density calibration (c).

305   designed to represent spatial and temporal evolution of firn density and surface height. On the other hand, SNOWPACK is a higher order complexity physics-based land-surface snow model originally intended for simulating snow microstructural properties relevant for avalanche formation in seasonally snow covered terrain. IMAU-FDM and GSFC-FDM are usually used to study the entire ice sheet firn column, which can be greater than 100 m thick, while SNOWPACK is typically used to simulate seasonal snowpacks a few meters thick. Despite the much thicker simulated firn column in IMAU-FDM and GSFC-

310   FDM (40 - 120 m) when compared to our imposed restriction for SNOWPACK to the near-surface (i.e. depths 0 - 10 m), SNOWPACK is considerably more computationally expensive to run. It is therefore important to acknowledge the inherent trade off between process representation and cost, particularly for simulations which require long spinups or involve long time frames, e.g. paleoclimate applications or future climate scenarios.

     Because SNOWPACK exhibits a lower mean snow and firn density bias throughout most of the near-surface compared

315   to IMAU-FDM and GSFC-FDM, it is necessary to describe particular model distinctions which could explain their different behavior. First, SNOWPACK and IMAU-FDM rely on different meteorological forcing (MERRA-2 and RACMO2 2.3p2, respectively) which somewhat confounds their direct comparison. Next, in our implementation of SNOWPACK, new snow density is determined by hourly mean MERRA-2 weather conditions while in IMAU-FDM and GSFC-FDM, new snow density is determined by annual average meteorologic variables including accumulation rate, 10 m wind speed, and surface temperature.

320   SNOWPACK therefore calculates a variable new snow density driven by both seasonal and synoptic scale variability in surface

meteorology, while IMAU-FDM and GSFC-FDM do not resolve this process. Additionally, SNOWPACK allows for drifting snow compaction of previously fallen snow (Fig. 1), while IMAU-FDM and GSFC-FDM only account for the impact of wind on density by including this processes in the new snow density parameterization. This difference in process representation of new snow density and drifting snow compaction is reflected by SNOWPACK's larger variability in predicted surface density

325   (281 - 479 $\mathrm{kg\,m^{-3}}$) comapred IMAU-FDM (328 - 429 $\mathrm{kg\,m^{-3}}$) and GSFC-FDM (364 - 436 $\mathrm{kg\,m^{-3}}$). By allowing for initial low density new snow accumulation and subsequent drifting snow compaction, SNOWPACK, more in line with observations (272 - 507 $\mathrm{kg\,m^{-3}}$), predicts a wider range of surface snow densities than IMAU-FDM and GSFC-FDM (Fig. 5, panels a, c, e). Finally, SNOWPACK's higher temporal resolution density output (daily) compared to IMAU-FDM (30 days) and GSFC-FDM (5 days), can resolve processes relevant for surface snow density which act on timescales of less than 30 and 5 days,

330   respectively (e.g. snowfall and drifting snow compaction).

3.7   Simulated snow cover properties for remote sensing interpretation

In addition to snow and firn density, SNOWPACK can be used to calculate other snow cover properties (e.g. snow grain diameter, temperature, albedo, and liquid water content) necessary for detailed interpretation of ice sheet remote sensing data. In Fig. 9, we provide an example of SNOWPACK simulated winter time temperature profiles and time series of 2010 - 2015

335   average surface (top 1 m) density and grain diameter at sites near the South Pole and WAIS. Note that due to limited available observations, we make no effort to validate these particular variables; instead, we merely offer them as a demonstration. As expected, South Pole is colder than WAIS throughout the entire near-surface, on average by 18.3 °C. WAIS surface density is on average 125 $\mathrm{kg\,m^{-3}}$ larger than that of South Pole while there is also significant predicted temporal variability of up to 16 % and 11 % of mean density for South Pole and WAIS, respectively. Additionally, surface grain diameter is larger at South

340   Pole while both sites show a large seasonal cycle, peaking in late summer and gradually declining throughout the winter.

By describing snow cover properties at South Pole (mean annual T_s = -52.4 °C and SMB = 56 $\mathrm{kg\,m^{-2}\,yr^{-1}}$) as well as WAIS (mean annual T_s = -29.4 °C and SMB = 207 $\mathrm{kg\,m^{-2}\,yr^{-1}}$), we present model evidence which demonstrates large regional variability in near-surface temperature as well as both regional and temporal variability in surface density and grain diameter. Although we do not directly evaluate simulated temporal variability in snow microstructural properties (e.g. surface

345   density and grain diameter) against temporally distributed observations, time series of simulated snow properties can be useful when developing new and or interpreting existing remote sensing observations.

4   Conclusions

Accurate snow and firn density models are required to reliably determine ice sheet mass balance using satellite altimetry. However, firn densification models currently used in altimetry studies do not resolve observed temporal increases in surface

350   snow density under the influence of wind. In this study, we demonstrate improved simulation of Antarctic near-surface (depths $\leq$ 10 m) snow and firn density upon implementation of a new drifting snow compaction routine into SNOWPACK, a detailed, physics-based land surface snow model. In particular, we show that when compared to two other semi-empirical firn densifica-
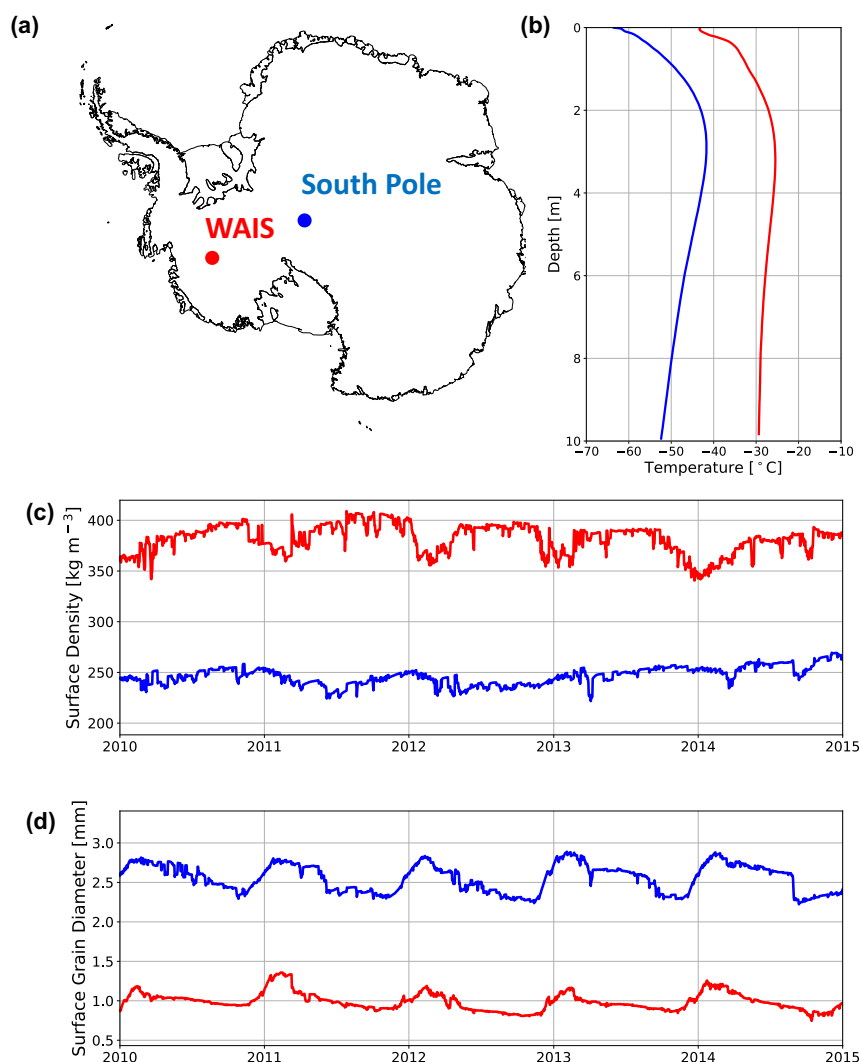
Figure 9. SNOWPACK simulated firn properties. Map indicating locations of South Pole and WAIS (a). SNOWPACK simulated near-surface temperature profiles (°C) at South Pole and WAIS on June 21, 2010 (b). Time series of 2010 - 2015 SNOWPACK simulated average surface density (kg m^{-3}) at South Pole and WAIS (c). Time series of 2010 - 2015 SNOWPACK simulated average surface grain diameter (mm) at South Pole and WAIS (d). In all panels South Pole is shown in blue and WAIS is shown in red.

tion models (IMAU-FDM and GSFC-FDM), SNOWPACK exhibits a lower mean snow and firn density bias throughout most of the near-surface at 122 observed density profiles across the Antarctic ice sheet. Despite this improvement, SNOWPACK

355 generally underestimates density, with a mean surface density bias of -8.2 kg m^{-3} and mean near-surface biases ranging from -0.6 kg m^{-3} at 2 - 3 m to -25.3 kg m^{-3} at 8 - 9 m. Meanwhile, IMAU-FDM exhibits a mean surface density bias of

-20.4 $\mathrm{kg\,m^{-3}}$ and mean near-surface biases between -20.4 $\mathrm{kg\,m^{-3}}$ at depths 0 - 1 m to -40.1 $\mathrm{kg\,m^{-3}}$ at depths 8 - 9 m while GSFC-FDM shows a mean surface density bias of 20.4 $\mathrm{kg\,m^{-3}}$ and mean near-surface biases from 8.5 $\mathrm{kg\,m^{-3}}$ at depths 8 - 9 m to 23.7 $\mathrm{kg\,m^{-3}}$ at 2 - 3 m. Because SNOWPACK is a physics-based model, extensive model tuning in order to fit obser-
360 vations is not required. For this reason, SNOWPACK, when compared to GSFC-FDM, more accurately simulates snow and firn density at sites whose density observations are not included in the GSFC-FDM density calibration. Because SNOWPACK outperforms the GSFC-FDM at sites not included in calibration, SNOWPACK, compared to semi-empirical models, may more reliably simulate firn density in regions without extensive observations and under future climate scenarios, where firn properties are expected to diverge from their current state.

365 *Code and data availability.* Upon publication, all software and code required to replicate this study will be made open-access at https://github.com/EricKeenan/Keenan_et_al_2020_TC. SNOWPACK model source code can be accessed at https://github.com/snowpack-model/snowpack, while the precise version used in this study can be accessed at https://doi.org/10.5281/zenodo.3891846. MERRA-2 atmospheric reanalysis is available at https://gmao.gsfc.nasa.gov/reanalysis/MERRA-2/ and can be retrieved and processed using our workflow available at https://github.com/EricKeenan/download_MERRA2. SUMup density data are available at https://arcticdata.io/catalog/view/doi:10.18739/
370 A26D5PB2S. Borehole 10 m depth temperature data are available from Michiel van den Broeke (m.r.vandenBroeke@uu.nl). AWS data are available from Carleen Reijmer (c.h.tijm-reijmer@uu.nl). IMAU-FDM data are available from Peter Kuipers Munneke (p.kuipersmunneke@uu.nl). GSFC-FDM data are available from Brooke Medley (brooke.c.medley@nasa.gov).

Appendix A

Author contributions. All authors contributed to preparing this manuscript. E.K. carried out SNOWPACK simulations, performed the anal-
375 ysis, and produced the figures. N.W. implemented the new drifting snow compaction routine into SNOWPACK and contributed to the experimental design and analysis. M.D and J.T.M.L. contributed to the experimental design and analysis. B.M. contributed to the experimental design and analysis and provided GSFC-FDM output. P.K.M provided IMAU-FDM output. C.R. provided AWS data.

Competing interests. The authors declare that they have no conflict of interest.

Acknowledgements. E.K., N.W., J.T.M.L., and B.M. acknowledge support from the National Aeronautics and Space Administration (NASA),
380 Grant 80NSSC18K0201 (ROSES-2016: studies with ICESat-2 and CryoSat-2). E.K., N.W., and J.T.M.L are also supported by BELSPO Research Contract, grant BR/165/A2:Mass2Ant. P.K.M. is funded by the Netherlands Earth System Science Centre (NESSC). C.R. acknowledges the support of the Dutch Polar program of the Dutch national research council NPP-NWO. This work utilized the RMACC Summit supercomputer, which is supported by the National Science Foundation (awards ACI-1532235 and ACI-1532236), the University of Colorado
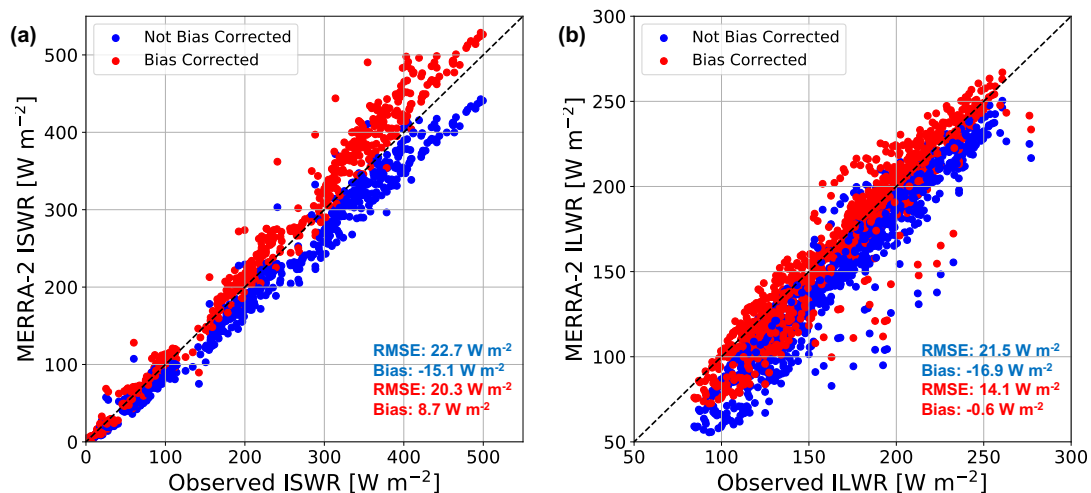
Figure A1. MERRA-2 incoming shortwave and longwave radiation bias correction. Comparison between monthly averaged AWS observed and MERRA-2 modeled incoming shortwave radiation (a) and longwave radiation (b) at nine automatic weather stations. Non-bias corrected MERRA-2 radiative fluxes are shown in blue while bias corrected fluxes are shown in red. Mean MERRA-2 root mean square error (RMSE, $W\,m^{-2}$) and bias ($W\,m^{-2}$) are shown in blue and red text for non bias corrected and bias corrected radiative fluxes, respectively. Dashed black line represents a one to one line.

Boulder, and Colorado State University. The Summit supercomputer is a joint effort of the University of Colorado Boulder and Colorado
385   State University. Data storage supported by the University of Colorado Boulder "PetaLibrary". The authors thank Lynn Montgomery for their
useful insight into the SUMup dataset and constructive comments on this manuscript.

References

Agosta, C., Amory, C., Kittel, C., Orsi, A., Favier, V., Gallée, H., van den Broeke, M. R., Lenaerts, J. T. M., van Wessem, J. M., van de Berg, W. J., and Fettweis, X.: Estimation of the Antarctic surface mass balance using the regional climate model MAR (1979–2015) and identification of dominant processes, The Cryosphere, 13, 281–296, https://doi.org/10.5194/tc-13-281-2019, https://www.the-cryosphere.net/13/281/2019/, 2019.

Albert, M.: Snow and Firn Permeability: Characteristics of Snow Megadunes and their Potential Effects on Ice Core Interpretation, https://doi.org/10.7265/N5639MPD, http://www.usap-dc.org/view/dataset/609299, type: dataset, 2007.

Alexander, P. M., Tedesco, M., Koenig, L., and Fettweis, X.: Evaluating a Regional Climate Model Simulation of Greenland Ice Sheet Snow and Firn Density for Improved Surface Mass Balance Estimates, Geophysical Research Letters, 46, 12 073–12 082, https://doi.org/10.1029/2019GL084101, https://onlinelibrary.wiley.com/doi/abs/10.1029/2019GL084101, 2019.

Amory, C. and Kittel, C.: Brief communication: Rare ambient saturation during drifting snow occurrences at a coastal location of East Antarctica, The Cryosphere, 13, 3405–3412, https://doi.org/10.5194/tc-13-3405-2019, https://www.the-cryosphere.net/13/3405/2019/, 2019.

Arthern, R. J., Vaughan, D. G., Rankin, A. M., Mulvaney, R., and Thomas, E. R.: In situ measurements of Antarctic snow compaction compared with predictions of models, Journal of Geophysical Research, 115, F03 011, https://doi.org/10.1029/2009JF001306, http://doi.wiley.com/10.1029/2009JF001306, 2010.

Bartelt, P. and Lehning, M.: A physical SNOWPACK model for the Swiss avalanche warning Part I: numerical model, Cold Regions Science and Technology, p. 23, 2002.

Brun, E., Martin, E., and Spiridonov, V.: Coupling a multi-layered snow model with a GCM, Annals of Glaciology, 25, 66–72, https://doi.org/10.3189/S0260305500013811, https://www.cambridge.org/core/product/identifier/S0260305500013811/type/journal_article, 1997.

Dattler, M. E., Lenaerts, J. T. M., and Medley, B.: Significant Spatial Variability in Radar-Derived West Antarctic Accumulation Linked to Surface Winds and Topography, Geophysical Research Letters, 46, 13 126–13 134, https://doi.org/10.1029/2019GL085363, https://onlinelibrary.wiley.com/doi/abs/10.1029/2019GL085363, 2019.

Dunmire, D., Lenaerts, J. T. M., Banwell, A. F., Wever, N., Shragge, J., Lhermitte, S., Drews, R., Pattyn, F., Hansen, J. S. S., Willis, I. C., Miller, J., and Keenan, E.: Observations of buried lake drainage on the Antarctic Ice Sheet, Geophysical Research Letters, https://doi.org/10.1029/2020GL087970, https://onlinelibrary.wiley.com/doi/abs/10.1029/2020GL087970, 2020.

Filhol, S. and Sturm, M.: Snow bedforms: A review, new data, and a formation model: Snow bedforms: Review and Modeling, Journal of Geophysical Research: Earth Surface, 120, 1645–1669, https://doi.org/10.1002/2015JF003529, http://doi.wiley.com/10.1002/2015JF003529, 2015.

Gelaro, R., McCarty, W., Suárez, M. J., Todling, R., Molod, A., Takacs, L., Randles, C. A., Darmenov, A., Bosilovich, M. G., Reichle, R., Wargan, K., Coy, L., Cullather, R., Draper, C., Akella, S., Buchard, V., Conaty, A., da Silva, A. M., Gu, W., Kim, G.-K., Koster, R., Lucchesi, R., Merkova, D., Nielsen, J. E., Partyka, G., Pawson, S., Putman, W., Rienecker, M., Schubert, S. D., Sienkiewicz, M., and Zhao, B.: The Modern-Era Retrospective Analysis for Research and Applications, Version 2 (MERRA-2), Journal of Climate, 30, 5419–5454, https://doi.org/10.1175/JCLI-D-16-0758.1, http://journals.ametsoc.org/doi/10.1175/JCLI-D-16-0758.1, 2017.

Gossart, A., Helsen, S., Lenaerts, J. T. M., Broucke, S. V., van Lipzig, N. P. M., and Souverijns, N.: An Evaluation of Surface Climatology in State-of-the-Art Reanalyses over the Antarctic Ice Sheet, Journal of Climate, 32, 6899–6915, https://doi.org/10.1175/JCLI-D-19-0030.1, http://journals.ametsoc.org/doi/10.1175/JCLI-D-19-0030.1, 2019.

Groot Zwaaftink, C. D., Cagnati, A., Crepaz, A., Fierz, C., Macelloni, G., Valt, M., and Lehning, M.: Event-driven deposition of snow on the
Antarctic Plateau: analyzing field measurements with SNOWPACK, The Cryosphere, 7, 333–347, https://doi.org/10.5194/tc-7-333-2013,
https://www.the-cryosphere.net/7/333/2013/, 2013.

Helm, V., Humbert, A., and Miller, H.: Elevation and elevation change of Greenland and Antarctica derived from CryoSat-2, The Cryosphere,
8, 1539–1559, https://doi.org/10.5194/tc-8-1539-2014, https://www.the-cryosphere.net/8/1539/2014/, 2014.

Herron, M. M. and Langway, C. C.: Firn Densification: An Empirical Model, Journal of Glaciology, 25, 373–385,
https://doi.org/10.3189/S0022143000015239, https://www.cambridge.org/core/product/identifier/S0022143000015239/type/journal_
article, 1980.

Izeboud, M., Lhermitte, S., Van Tricht, K., Lenaerts, J. T. M., Van Lipzig, N. P. M., and Wever, N.: The spatiotemporal variability of cloud
radiative effects on the Greenland Ice Sheet surface mass balance, Geophysical Research Letters, https://doi.org/10.1029/2020GL087315,
https://onlinelibrary.wiley.com/doi/abs/10.1029/2020GL087315, 2020.

Jakobs, C. L., Reijmer, C. H., Smeets, C. J. P. P., Trusel, L. D., van de Berg, W. J., van den Broeke, M. R., and van Wessem, J. M.: A benchmark
dataset of in situ Antarctic surface melt rates and energy balance, Journal of Glaciology, 66, 291–302, https://doi.org/10.1017/jog.2020.6,
https://www.cambridge.org/core/product/identifier/S0022143020000064/type/journal_article, 2020.

Kausch, T., Lhermitte, S., Lenaerts, J. T. M., Wever, N., Inoue, M., Pattyn, F., Sun, S., Wauthy, S., Tison, J.-L., and van de Berg, W. J.:
Impact of coastal East Antarctic ice rises on surface mass balance: insights from observations and modeling, preprint, Ice sheets/Antarctic,
https://doi.org/10.5194/tc-2020-66, https://www.the-cryosphere-discuss.net/tc-2020-66/, 2020.

Kuipers Munneke, P., Ligtenberg, S. R. M., Noël, B. P. Y., Howat, I. M., Box, J. E., Mosley-Thompson, E., McConnell, J. R., Steffen, K.,
Harper, J. T., Das, S. B., and van den Broeke, M. R.: Elevation change of the Greenland Ice Sheet due to surface mass balance and firn
processes, 1960–2014, The Cryosphere, 9, 2009–2025, https://doi.org/10.5194/tc-9-2009-2015, https://www.the-cryosphere.net/9/2009/
2015/, 2015.

Lehning, M. and Fierz, C.: Assessment of snow transport in avalanche terrain, Cold Regions Science and Technology, 51, 240–252,
https://doi.org/10.1016/j.coldregions.2007.05.012, https://linkinghub.elsevier.com/retrieve/pii/S0165232X0700122X, 2008.

Lehning, M., Bartelt, P., Brown, B., and Fierz, C.: A physical SNOWPACK model for the Swiss avalanche warning Part III: meteorological
forcing, thin layer formation and evaluation, Cold Regions Science and Technology, p. 16, 2002a.

Lehning, M., Bartelt, P., Brown, B., Fierz, C., and Satyawali, P.: A physical SNOWPACK model for the Swiss avalanche warning Part II.
Snow microstructure, Cold Regions Science and Technology, p. 21, 2002b.

Lenaerts, J. T. M., van den Broeke, M. R., Déry, S. J., van Meijgaard, E., van de Berg, W. J., Palm, S. P., and Sanz Rodrigo, J.: Modeling
drifting snow in Antarctica with a regional climate model: 1. Methods and model evaluation: DRIFTING SNOW IN ANTARCTICA,
1, Journal of Geophysical Research: Atmospheres, 117, n/a–n/a, https://doi.org/10.1029/2011JD016145, http://doi.wiley.com/10.1029/
2011JD016145, 2012.

Lenaerts, J. T. M., Medley, B., Broeke, M. R., and Wouters, B.: Observing and Modeling Ice Sheet Surface Mass Balance, Reviews of Geo-
physics, 57, 376–420, https://doi.org/10.1029/2018RG000622, https://onlinelibrary.wiley.com/doi/abs/10.1029/2018RG000622, 2019.

Li, J. and Zwally, H. J.: Modeling of firn compaction for estimating ice-sheet mass change from observed ice-sheet elevation
change, Annals of Glaciology, 52, 1–7, https://doi.org/10.3189/172756411799096321, https://www.cambridge.org/core/product/identifier/
S0260305500250921/type/journal_article, 2011.

Ligtenberg, S. R. M., Helsen, M. M., and van den Broeke, M. R.: An improved semi-empirical model for the densification of Antarctic firn,
The Cryosphere, 5, 809–819, https://doi.org/10.5194/tc-5-809-2011, https://www.the-cryosphere.net/5/809/2011/, 2011.

Ligtenberg, S. R. M., Kuipers Munneke, P., and van den Broeke, M. R.: Present and future variations in Antarctic firn air content, The Cryosphere, 8, 1711–1723, https://doi.org/10.5194/tc-8-1711-2014, https://www.the-cryosphere.net/8/1711/2014/, 2014.

Ligtenberg, S. R. M., Kuipers Munneke, P., Noël, B. P. Y., and van den Broeke, M. R.: Brief communication: Improved simulation of the
465 present-day Greenland firn layer (1960–2016), The Cryosphere, 12, 1643–1649, https://doi.org/10.5194/tc-12-1643-2018, https://www.the-cryosphere.net/12/1643/2018/, 2018.

Medley, B. and Thomas, E. R.: Increased snowfall over the Antarctic Ice Sheet mitigated twentieth-century sea-level rise, Nature Climate Change, 9, 34–39, https://doi.org/10.1038/s41558-018-0356-x, http://www.nature.com/articles/s41558-018-0356-x, 2019.

Medley, B., Joughin, I., Das, S. B., Steig, E. J., Conway, H., Gogineni, S., Criscitiello, A. S., McConnell, J. R., Smith, B. E., van den
470 Broeke, M. R., Lenaerts, J. T. M., Bromwich, D. H., and Nicolas, J. P.: Airborne-radar and ice-core observations of annual snow accumulation over Thwaites Glacier, West Antarctica confirm the spatiotemporal variability of global and regional atmospheric models: SNOW ACCUMULATION OVER THWAITES GLACIER, Geophysical Research Letters, 40, 3649–3654, https://doi.org/10.1002/grl.50706, http://doi.wiley.com/10.1002/grl.50706, 2013.

Medley, B., McConnell, J. R., Neumann, T. A., Reijmer, C. H., Chellman, N., Sigl, M., and Kipfstuhl, S.: Temperature and Snow-
475 fall in Western Queen Maud Land Increasing Faster Than Climate Model Projections, Geophysical Research Letters, 45, 1472–1480, https://doi.org/10.1002/2017GL075992, https://onlinelibrary.wiley.com/doi/abs/10.1002/2017GL075992, 2018.

Medley, B., T.A., N., and Zwally, H.: Forty-year Simulations of Firn Processes over the Greenland and Antarctic Ice Sheets., Submitted to Earth and Space Sciences., 2020.

Montgomery, L., Koenig, L., and Alexander, P.: The SUMup dataset: compiled measurements of surface mass balance components over ice
480 sheets and sea ice with analysis over Greenland, Earth System Science Data, 10, 1959–1985, https://doi.org/10.5194/essd-10-1959-2018, https://www.earth-syst-sci-data.net/10/1959/2018/, 2018.

Montgomery, L., Koenig, L., Lenaerts, J. T. M., and Kuipers Munneke, P.: Accumulation rates (2009–2017) in Southeast Greenland derived from airborne snow radar and comparison with regional climate models, Annals of Glaciology, pp. 1–9, https://doi.org/10.1017/aog.2020.8, https://www.cambridge.org/core/product/identifier/S0260305520000087/type/journal_article, 2020.

485 Palm, S. P., Kayetha, V., Yang, Y., and Pauly, R.: Blowing snow sublimation and transport over Antarctica from 11 years of CALIPSO observations, The Cryosphere, 11, 2555–2569, https://doi.org/10.5194/tc-11-2555-2017, https://www.the-cryosphere.net/11/2555/2017/, 2017.

Picard, G., Arnaud, L., Caneill, R., Lefebvre, E., and Lamare, M.: Observation of the process of snow accumulation on the Antarctic Plateau by time lapse laser scanning, The Cryosphere, 13, 1983–1999, https://doi.org/10.5194/tc-13-1983-2019, https://www.the-cryosphere.net/
490 13/1983/2019/, 2019.

Reijmer, C. H.: Temporal and spatial variability of the surface energy balance in Dronning Maud Land, East Antarctica, Journal of Geophysical Research, 107, 4759, https://doi.org/10.1029/2000JD000110, http://doi.wiley.com/10.1029/2000JD000110, 2002.

Rignot, E., Mouginot, J., Scheuchl, B., van den Broeke, M., van Wessem, M. J., and Morlighem, M.: Four decades of Antarctic Ice Sheet mass balance from 1979–2017, Proceedings of the National Academy of Sciences, 116, 1095–1103, https://doi.org/10.1073/pnas.1812883116,
495 http://www.pnas.org/lookup/doi/10.1073/pnas.1812883116, 2019.

Shepherd, A., Ivins, E. R., A, G., Barletta, V. R., Bentley, M. J., Bettadpur, S., Briggs, K. H., Bromwich, D. H., Forsberg, R., Galin, N., Horwath, M., Jacobs, S., Joughin, I., King, M. A., Lenaerts, J. T. M., Li, J., Ligtenberg, S. R. M., Luckman, A., Luthcke, S. B., McMillan, M., Meister, R., Milne, G., Mouginot, J., Muir, A., Nicolas, J. P., Paden, J., Payne, A. J., Pritchard, H., Rignot, E., Rott, H., Sorensen, L. S., Scambos, T. A., Scheuchl, B., Schrama, E. J. O., Smith, B., Sundal, A. V., van Angelen, J. H., van de Berg, W. J., van den Broeke, M. R.,

500   Vaughan, D. G., Velicogna, I., Wahr, J., Whitehouse, P. L., Wingham, D. J., Yi, D., Young, D., and Zwally, H. J.: A Reconciled Estimate of Ice-Sheet Mass Balance, Science, 338, 1183–1189, https://doi.org/10.1126/science.1228102, https://www.sciencemag.org/lookup/doi/10.1126/science.1228102, 2012.

Smith, B., Fricker, H. A., Gardner, A. S., Medley, B., Nilsson, J., Paolo, F. S., Holschuh, N., Adusumilli, S., Brunt, K., Csatho, B., Harbeck, K., Markus, T., Neumann, T., Siegfried, M. R., and Zwally, H. J.: Pervasive ice sheet mass loss reflects competing ocean and

505   atmosphere processes, Science, p. eaaz5845, https://doi.org/10.1126/science.aaz5845, https://www.sciencemag.org/lookup/doi/10.1126/science.aaz5845, 2020.

Sommer, C. G., Lehning, M., and Fierz, C.: Wind tunnel experiments: saltation is necessary for wind-packing, Journal of Glaciology, 63, 950–958, https://doi.org/10.1017/jog.2017.53, https://www.cambridge.org/core/product/identifier/S0022143017000533/type/journal_article, 2017.

510   Sommer, C. G., Wever, N., Fierz, C., and Lehning, M.: Investigation of a wind-packing event in Queen Maud Land, Antarctica, The Cryosphere, 12, 2923–2939, https://doi.org/10.5194/tc-12-2923-2018, https://www.the-cryosphere.net/12/2923/2018/, 2018.

Steger, C. R., Reijmer, C. H., van den Broeke, M. R., Wever, N., Forster, R. R., Koenig, L. S., Kuipers Munneke, P., Lehning, M., Lhermitte, S., Ligtenberg, S. R. M., Miège, C., and Noël, B. P. Y.: Firn Meltwater Retention on the Greenland Ice Sheet: A Model Comparison, Frontiers in Earth Science, 5, https://doi.org/10.3389/feart.2017.00003, http://journal.frontiersin.org/article/10.3389/feart.2017.00003/full, 2017.

515   Stevens, C. M., Verjans, V., Lundin, J. M., Kahle, E. C., Horlings, A. N., Horlings, B. I., and Waddington, E. D.: The Community Firn Model (CFM) v1.0, preprint, Cryosphere, https://doi.org/10.5194/gmd-2019-361, https://www.geosci-model-dev-discuss.net/gmd-2019-361/, 2020.

The IMBIE team: Mass balance of the Antarctic Ice Sheet from 1992 to 2017, Nature, 558, 219–222, https://doi.org/10.1038/s41586-018-0179-y, http://www.nature.com/articles/s41586-018-0179-y, 2018.

520   Trusel, L. D., Frey, K. E., Das, S. B., Munneke, P. K., and van den Broeke, M. R.: Satellite-based estimates of Antarctic surface meltwater fluxes: SATELLITE-BASED ANTARCTIC MELT FLUXES, Geophysical Research Letters, 40, 6148–6153, https://doi.org/10.1002/2013GL058138, http://doi.wiley.com/10.1002/2013GL058138, 2013.

van den Broeke, M.: Depth and Density of the Antarctic Firn Layer, Arctic, Antarctic, and Alpine Research, 40, 432–438, https://doi.org/10.1657/1523-0430(07-021)[BROEKE]2.0.CO;2, http://www.bioone.org/doi/abs/10.1657/1523-0430%2807-021%

525   29%5BBROEKE%5D2.0.CO%3B2, 2008.

van Kampenhout, L., Lenaerts, J. T. M., Lipscomb, W. H., Sacks, W. J., Lawrence, D. M., Slater, A. G., and van den Broeke, M. R.: Improving the Representation of Polar Snow and Firn in the Community Earth System Model: IMPROVING POLAR SNOW AND FIRN IN CESM, Journal of Advances in Modeling Earth Systems, 9, 2583–2600, https://doi.org/10.1002/2017MS000988, http://doi.wiley.com/10.1002/2017MS000988, 2017.

530   Van Tricht, K., Lhermitte, S., Lenaerts, J. T. M., Gorodetskaya, I. V., L'Ecuyer, T. S., Noël, B., van den Broeke, M. R., Turner, D. D., and van Lipzig, N. P. M.: Clouds enhance Greenland ice sheet meltwater runoff, Nature Communications, 7, 10 266, https://doi.org/10.1038/ncomms10266, http://www.nature.com/articles/ncomms10266, 2016.

van Wessem, J. M., Reijmer, C. H., Lenaerts, J. T. M., van de Berg, W. J., van den Broeke, M. R., and van Meijgaard, E.: Updated cloud physics in a regional atmospheric climate model improves the modelled surface energy balance of Antarctica, The Cryosphere, 8, 125–135,

535   https://doi.org/10.5194/tc-8-125-2014, https://www.the-cryosphere.net/8/125/2014/, 2014.

van Wessem, J. M., van de Berg, W. J., Noël, B. P. Y., van Meijgaard, E., Amory, C., Birnbaum, G., Jakobs, C. L., Krüger, K., Lenaerts, J. T. M., Lhermitte, S., Ligtenberg, S. R. M., Medley, B., Reijmer, C. H., van Tricht, K., Trusel, L. D., van Ulft, L. H., Wouters, B., Wuite,

J., and van den Broeke, M. R.: Modelling the climate and surface mass balance of polar ice sheets using RACMO2 – Part 2: Antarctica (1979–2016), The Cryosphere, 12, 1479–1498, https://doi.org/10.5194/tc-12-1479-2018, https://www.the-cryosphere.net/12/1479/2018/, 2018.

540

Vionnet, V., Brun, E., Morin, S., Boone, A., Faroux, S., Le Moigne, P., Martin, E., and Willemet, J.-M.: The detailed snowpack scheme Crocus and its implementation in SURFEX v7.2, Geoscientific Model Development, 5, 773–791, https://doi.org/10.5194/gmd-5-773-2012, https://www.geosci-model-dev.net/5/773/2012/, 2012.

Weinhart, A. H., Freitag, J., Hörhold, M., Kipfstuhl, S., and Eisen, O.: Representative surface snow density on the East Antarctic Plateau,

545

preprint, Snow/Antarctic, https://doi.org/10.5194/tc-2020-14, https://www.the-cryosphere-discuss.net/tc-2020-14/, 2020.

Zwally, H. J., Li, J., Robbins, J. W., Saba, J. L., Yi, D., and Brenner, A. C.: Mass gains of the Antarctic ice sheet exceed losses, Journal of Glaciology, 61, 1019–1036, https://doi.org/10.3189/2015JoG15J071, https://www.cambridge.org/core/product/identifier/S0022143000200221/type/journal_article, 2015.